Agent-Based Simulation of Drug Disposition in Cirrhotic Liver

Sean H. J. Kim[1], Sunwoo Park[2], Glen E. P. Ropella[2], and C. Anthony Hunt[1,2]

[1] **Joint Graduate Group in Bioengineering, University of California, Berkeley and San Francisco, CA 94720, USA**
[2] **Department of Bioengineering and Therapeutic Sciences, University of California, San Francisco, CA 94143, USA**

seanhjk@berkeley.edu parks@pharmacy.ucsf.edu gepr@tempusdictum.com a.hunt@ucsf.edu

Keywords: in silico liver, drug disposition, cirrhosis, multi-scale tracing

Abstract

Cirrhosis, a chronic liver disease, alters hepatic drug disposition. Little is known about mechanisms underpinning the disease progression and how they contribute to changes in liver disposition properties. Here we present multilevel, agent-based and agent-directed In Silico Livers (ISLs) to probe plausible answers for a cationic drug, diltiazem, in two different types of cirrhotic rat livers. Starting with ISLs that validated against diltiazem disposition data from normal livers, we systematically transformed ISL characteristics to achieve validation against perfusion outflow profiles from the two types of diseased livers. For detailed analysis, we developed and implemented methods to trace each object representing diltiazem during simulated perfusion experiments. So doing enabled gaining heretofore-unavailable insight into plausible disposition details from diltiazem perspective in normal and diseased livers. From the results, we posit that changes in ISL micromechanistic details may have disease caused counterparts during disposition.

1. INTRODUCTION

Cirrhosis includes chronic, advanced fibrosis (scarring) of liver, a major site of drug metabolism and clearance. It results from the perpetuation of the normal wound healing response and subsequent distortion of hepatic histoarchitecture. The disease complicates drug therapy management because it alters hepatic drug disposition, which, in turn, alters pharmacokinetic (PK) and/or pharmacodynamic (PD) characteristics. The nature of alteration is dependent on both the nature and the extent of disease. With some exceptions (e.g., [1]), little is known about exactly how the cirrhotic changes affect hepatic drug disposition. Improved, mechanistic insight is needed to enable rational drug therapy based on clinical measures of both type and extent of liver disease.

Here we report further progress in understanding drug disposition in cirrhotic liver by developing and experimenting on multi-scale In Silico Livers (ISLs) [2]. Key ISL and support components were represented as independent, interacting agents. In silico experiments were conducted using an automated, high-performance software environment capable of parallel computation. For this study we started with ISLs that validated for drug and sucrose disposition profiles of normal rat livers in situ [3]. The models were then subjected to cycles of experimentation and iterative refinement to achieve simulated drug disposition profiles that were acceptably similar to those from two different types of diseased livers [1]. The diseased ISLs were created independently: for each type, an increasing number of normal ISL characteristics were altered systematically until simulated drug disposition profiles were experimentally indistinguishable from the referent profiles.

Having achieved validation, we posit that the causative, mechanistic details occurring during ISL execution may have wet-lab hepatic counterparts during disposition, as diagrammed in Fig. 1. Differences in mechanistic details between the normal and the two "diseased" ISLs are hypotheses about corresponding differences between the normal and diseased livers, and about differences between diseased livers. Achieving a degree of profile similarity is evidence supporting those hypotheses. The differences in dynamic, multilevel details during execution of the two diseased ISLs provide a plausible, physiologically based explanation of the disease-caused differences in hepatic drug disposition. We expect that with additional rounds of refinement and validation, ISLs will provide increasingly useful scientific predictions and deeper insight into mechanistic details of disease progression and its role in hepatic PK.

2. BIOLOGY

2.1. Liver and Cirrhosis

Liver is the largest glandular organ (~1.5 kg; human), which plays a central role in drug metabolism and clearance. Cells composing the liver, called hepatocytes, are organized into roughly hexagonal units called lobules. Each lobule is centered around a central vein that drains blood into the hepatic vein. Along its periphery, a lobule is associated with hepatic portal vein and artery networks. Vessels, lined by

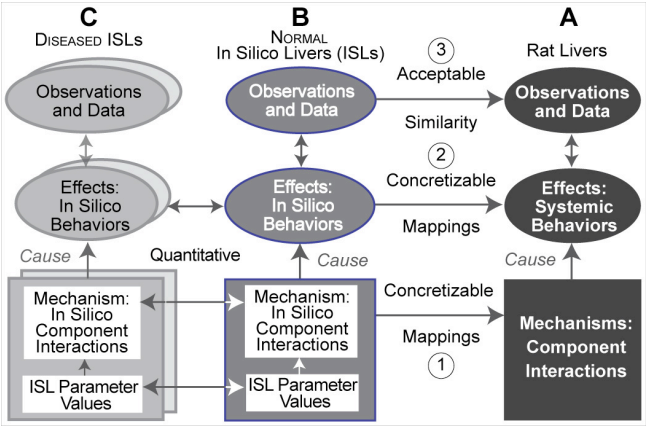

Figure 1. Relationships between perfused rat liver models and In Silico Livers (ISLs). **(A)** Perfused rat livers in their experimental context are the referent systems. During experiments, liver components interact with transiting drug molecules causing changes in the compound's outflow profile. Systemic behaviors at all levels are reflected in the collected data. **(B)** ISL components are designed, coded, verified, and assembled based on mechanism and component descriptions that are physiologically based. Concretizable mapping 1 is intended to exist from ISL components and interactions to hepatic physiological and microanatomic details. System dynamics during execution (mapping 2) are intended to abstractly represent plausible corresponding dynamics occurring within the liver during disposition. Measures of dynamics provide time series data that are intended to mimic counterpart measures of wet-lab perfusion experiments. Achieving measurable similarities makes mapping 3 quantitative. **(C)** Diseased counterparts to normal ISLs can be achieved by iteratively altering a subset of normal parameter values, mechanisms, and events into diseased counterparts that validate. Conceptual mappings are offered to relate differences in parameter values (normal to diseased) to measures of histopathology.

endothelial cells, branch among the hepatocytes, forming sinusoids into which the blood flows.

Cirrhosis distorts hepatic tissue architecture and vasculature [4]. Loss of endothelial fenestrations and filling of the space of Disse, a permeable connective tissue interface between endothelia and hepatocytes, can be observed as disease progresses. Various factors such as chronic alcoholism and hepatitis contribute to cirrhotic development. Major clinical consequences include impaired hepatocyte (liver) function, alterations in drug disposition, and circulatory abnormalities. Currently available therapeutic treatments primarily focus on reducing complications and preventing further degeneration.

2.2. In Situ Liver Perfusion

Full details of the original single-pass perfusion experiments are provided in [1]. Normal livers and two types of cirrhotic liver were studied. Both diseased types followed a similar pretreatment protocol to induce cirrhotic changes: one was produced by chronic carbon tetrachloride (CCl_4) treatment; the other was by chronic alcohol (ethanol) treatment. Both treatments induced hepatic injury, but their histologies were different. Chronic CCl_4 treatment produced acute hepatocellular injury with centrilobular necrosis and stenosis, whereas alcohol treatment resulted in hepatocellular injury with inflammation and perivenular degeneration. Control, normal PK profiles were obtained using livers from matched rats treated identically, absent either CCl_4 or alcohol treatment. Nine outflow profiles of diltiazem were analyzed individually using established PK methods.

3. MODEL

3.1. In Silico Liver

Detailed descriptions of ISL design and the mappings between ISL components and mechanisms and liver histology and physiology are available in [2], [3], [5]. To clearly distinguish in silico components and processes from corresponding hepatic structures and processes, hereafter we use small caps when referring to the ISL counterparts.

An ISL simulation framework corresponds to an entire wet-lab experimental system. It comprises an experiment agent, which is a highly abstract analogue of the scientists conducting liver perfusion experiments, a data management module, a statistical observer module, a parameter manager, and three different models: *DatModel*, *RefModel*, and *ArtModel*. *DatModel* is the referent data from [1]. *RefModel* is a classical, two-phase stochastic PK model fitted to *DatModel* [1]. The fitted model predicts the time course of diltiazem in liver effluent during a perfusion experiment.

ArtModel is the complete system illustrated in Fig. 2. As in [2], [3], [5], we assumed that anatomical and physiological characteristics of all hepatic lobules, normal and diseased, are somewhat similar. Each LIVER is thus a collection of similar LOBULES. However, a collection of heterogeneous LOBULES can be easily implemented, should that be required. To represent a single outflow profile, we pool results from ISL executions of 48 Monte Carlo variants of a single, parameterized LOBULE; those pooled, averaged results comprise one in silico LIVER PERFUSION experiment. Hereafter, ISL and LIVER are used interchangeably.

3.2. LOBULAR Components

The relative arrangement of hepatic function and flow is represented at the LOBULE level using a directed graph called sinusoid network. Each Monte Carlo variant of a network maps to a distinct arrangement of flow paths from portal vein tracts (PV) to the lobular central vein (CV) within an acinus. A sinusoid network is subdivided into three zones. The number of nodes per zone is always Zone I > Zone II > Zone III. Zone I, being close to PV, always

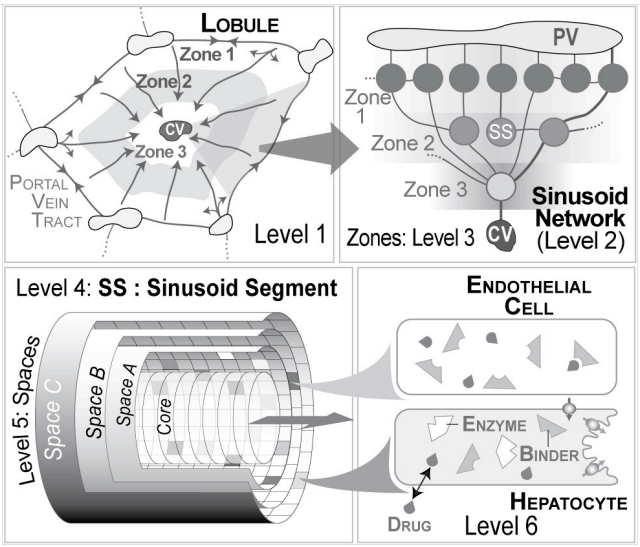

Figure 2. Hierarchical, multilevel structure of an In Silico Liver (ISL). A LOBULE maps to the functional unit of the liver, which consists of portal vein tracts (PV), a central vein (CV), and interconnected sinusoids. Blood flows from PV to CV. A LOBULE network is specified using an interconnected directed graph having Sinusoidal Segment (SS) nodes organized into three zones. Intra-zonal connections are possible. Inter-zone connections link SS nodes from Zone 1 to 2, from 1 to 3, and from 2 to 3. A SS maps to a unit of sinusoid structure and function. It contains a Core and three two-dimensional toroidal grid spaces. Space A maps to the interface between blood flow and cells. Space B is the ENDOTHELIAL layer, which comprises ENDOTHELIAL CELLS and spaces in-between. Space C is called the HEPATOCYTE layer; it contains HEPATOCYTES and EXTRACELLULAR spaces. ENDOTHELIAL CELLS and HEPATOCYTES contain BINDERS that can bind COMPOUNDS. BINDERS in HEPATOCYTES function as METABOLIZING ENZYMES. Objects representing DRUG move within and between spaces; DRUG can move in and out of CELLS.

has more nodes; Zone III, being next to CV, has the fewest. Zonation enables mimicking quantitative and functional differences between periportal and perivenous lobular regions [6]. A graph edge specifies a flow connection between two nodes. Lobular variability within and between livers is simulated by having edges assigned pseudo-randomly at the start of each of the 48 LOBULAR runs.

A Sinusoidal Segment (SS) is a software agent that represents all aspects of sinusoid function that can influence drug disposition. One SS is assigned to each graph node. Each SS is somewhat different and the stochastic differences are parameter controlled. SS counts per zone were Zone I = 45, Zone II = 20, and Zone III = 5. As explained in [5], these numbers were needed for sufficient PV-to-CV path variety to reduce fluctuations within outflow profiles. The SSs were connected using a minimum of 109 edges: 39 intra-Zone I edges, 8 intra-Zone II connections, 37 Zone I-to-Zone II, and 25 Zone II-to-Zone III connections. All Zone III nodes were connected to CV. Two SS types were used: direct (larger, shorter; controlled by the *DirSin* parameters) and tortuous (thinner, longer; controlled by the *TortSin* parameters).

A SS consists of a Core and three layered toroidal spaces, as illustrated in Fig. 2. The Core maps to blood flow. It provides a direct PV-to-CV path through which COMPOUNDS (mobile objects) can traverse. Spaces A–C have the same dimensions. The spaces are subdivided into a parameter specified number of square grid sites. Space A maps to the interface between vascular blood flow and the endothelial layer. Space B is called the ENDOTHELIAL layer. It maps to easily accessible spaces and cells presumed to be primarily endothelial cells. Space C is called the HEPATOCYTE layer. It maps to less accessible spaces and cells, primarily the space of Disse, hepatocytes, and bile canaliculi. CELLS in Space B are called ENDOTHELIAL CELLS; those in Space C are called HEPATOCYTES. Parameters allow the resolution of the spaces to be increased (or decreased) as needed. Grid space sizes are the same as in [3], [5].

CELLS contain objects that are needed to represent required intracellular processes such as drug binding, metabolism, transport, and sequestration. Because the in situ perfusions had short durations (less than one hour), we assumed that cell biology and biochemistry were relatively constant. Consequently, those details have been abstracted away, but can be added easily when needed without having to reengineer ISL. It is known that basic compounds such as diltiazem are sequestered in organelles such as lysosomes and mitochondria, as well as being bound [1], [7]. However, motivated by parsimony, sequestration and binding were not resolved: everything within a cell that can bind or sequester diltiazem is conflated and represented by some number of identical binding objects (hereafter, simply BINDERS). BINDERS inside HEPATOCYTES are called ENZYMES, and their BINDING events can end with release of METABOLITES.

3.3. ISL Parameters

ISL parameters specify structural and functional properties, experiment configuration, and dosage characteristics. We used the same set of parameters detailed in [2].

One ISL simulation experiment averages 48 Monte Carlo runs (or executions) using one LOBULE. The duration of each execution is specified by *cycleLimit*. The number of steps executed each cycle is *stepsPerCycle*. The execution-cycle-step hierarchy enabled observing and analyzing ISL experiments using two time resolutions. DRUG disposition is observed at cycle resolution; spatiotemporal activities are traced at step resolution. One simulation cycle maps to 0.5 seconds, the finest resolution of the validation data. *CycleLimit* and *stepsPerCycle* were set to 200 and 2, respectively.

Parameters described below govern structural and spatiotemporal properties of Sinusoidal Segments and components at lower ISL levels. *DirSinRatio* and *TortSinRatio* specify the ratio of the two SS types. SS circumference and length are generated using the values of *DirSinCircMin*, *DirSinCircMax*, *TortSinCircMin*, *TortSinCircMax*, *DirSinLenAlpha*, *DirSinLenBeta*, *DirSinLenShift*, *TortSinLenAlpha*, *TortSinLenBeta*, and *TortSinLenShift*. COMPOUND movements from one SS space to another are governed by *A2BJumpProb*, *B2AJumpProb*, *B2CJumpProb*, and *C2BJumpProb*. Simulated blood flow (in the Core) and local, biased random walk (Spaces A-C) are controlled by *CoreFlowRate* and *SinusoidTurbo*; their values can depend on the COMPOUND'S physicochemical properties. *ECDensity* and *HepDensity* specify the number of ENDOTHELIAL CELLS and HEPATOCYTES in Spaces B and C, respectively. The number of BINDERS in a CELL is Monte Carlo determined and is within the range specified by *BindersPerCellMin* and *BindersPerCellMax*. *SoluteBindingProb* specifies the probability of BINDING for a COMPOUND located within a BINDER'S local neighborhood. *SoluteBindingCycle* sets the duration of each BINDING event. The latter two parameters also depend on the COMPOUND'S physicochemical properties.

A set of parameters defines COMPOUND properties and characteristics. *MetabolizeProb* is the probability that a METABOLITE, rather than its parent COMPOUND, will be released from an ENZYME-COMPOUND complex. *ISLWetLabScaling* is a scaling factor used to map COMPOUNDS exiting CV directly to perfusate concentration in situ. *MembraneCrossing* is a binary property of each COMPOUND, which specifies whether that particular COMPOUND can enter CELLS.

3.4. COMPOUND Disposition

We describe LIVER disposition functions from the perspective of a COMPOUND traversing through a LOBULE. At the start of simulation, a parameter specified number of COMPOUNDS is instantiated and placed in PV. Initially these COMPOUNDS move into connected SSs through the Core and Space A. Their movement is biased random walk toward CV. At any time, a COMPOUND can move (jump) from Space A to B, or from B to C, or vice versa with a parameter specified probability (*A2BJumpProb*, *B2AJumpProb*, *B2CJumpProb*, or *C2BJumpProb*). A COMPOUND positioned next to a HEPATOCYTE or ENDOTHELIAL CELL can be taken up by (i.e., TRANSPORT into) the CELL. A CELL contains some number of BINDERS, one of which binds the TRANSPORTED COMPOUND with a parameter specified probability (*SoluteBindingProb*). BINDERS inside HEPATOCYTES can METABOLIZE the COMPOUND and release a METABOLITE. For all other BINDING events, the COMPOUND is released after parameter specified duration (*SoluteBindingCycle*). The released COMPOUND continues its travel through linked SSs and between SS spaces until it reaches CV, at which point the COMPOUND is collected and removed from the system.

3.5. Multi-Scale Event Tracing

Tracing disposition events within and between ISL levels was divided into two phases: generating raw tracing data and then aggregating the data using a set of quantitative measures.

In the first phase, all spatiotemporal events involving COMPOUNDS (of the same type) and their interactions with ISL components across all ISL levels were recorded. A trace data file was generated for each SS including PV and CV, which tracked the temporal order of events involving COMPOUNDS that resided within that SS. To trace METABOLIC events, each SS also generated a tracing file that listed the COMPOUND'S ID and type along with the TIME METABOLISM occurred.

In the second phase, collected raw data were reorganized and translated into analytical tracing measures for evaluation. We started by tracing changes at Levels 1 and 2 (Fig. 2): changes associated with ENDOTHELIAL CELLS, HEPATOCYTES, ENZYMES, and BINDERS at Level 1 and within the four SS spaces. Tracing results at higher levels were deduced by aggregating results from lower levels. Tracing measures included the path traversed by each COMPOUND, a COMPOUND'S resident TIME within an ISL or one of its features, and the fraction of BOUND or UNBOUND COMPOUNDS in each SS. Those measures were used to assess how mechanisms of COMPOUND disposition differed between NORMAL and DISEASED LIVERS.

3.6. Similarity Measure

ISL outflow profiles were compared with referent profiles using the quantitative Similarity Measure defined previously [2], [3], [5]. An ISL outflow profile was accepted as valid—as being indistinguishable experimentally from an in situ profile—when SM > 0.9. The SM measures the fraction of collected COMPOUNDS that lies within a band that was a prespecified, scaled factor of referent outflow values:

$$SM_1(p_s, p_r, s, e, k) = \frac{\sum_{i=s}^{e} \mathcal{C}(p_r^l(i,k) \le p_s(i) \le p_r^u(i,k))}{(e-s+1)} \quad (1)$$

where p_s: simulated hepatic disposition outflow profile; p_r: in situ hepatic disposition outflow profile; $s,e \in \boldsymbol{Z}^+$: start and end simulation cycle number; μ: sample mean of p_r; $\gamma_r = (p_r - \mu)/\mu$; $k \in \boldsymbol{R}^+$: scaling factor of the $\pm k \cdot \sigma(\gamma_r)$ band; $p_r^l(i,k) = p(i)(1 - k \cdot \sigma(\gamma_r))$: lower bound of the band; $p_r^u(i,k) = p(i)(1 + k \cdot \sigma(\gamma_r))$: upper bound of the band; $\sigma(\gamma_r)$: standard deviation of γ_r; $C(cond) = 1$ if the *cond* is true, otherwise 0; and $k = 0.5$, 0.75, or 1.0. Both raw and smoothed ISL profiles were scored.

4. RESULTS

4.1. Model Validation

Starting with validated NORMAL ISLs [2], [3] and the diltiazem outflow profiles from a CCl_4-treated liver as referents, we iteratively adjusted NORMAL ISL parameter values to change the properties of DILTIAZEM outflow profiles. We continued that adjustment process until the outflow profile achieved SM > 0.9. The resulting, validated ISL was called DISEASED_{CCl4} ISL. We then repeated that same protocol with the diltiazem outflow profiles from an alcohol-treated liver as the referent. ISL that achieved validation was called DISEASED_{ALC} ISL.

Table 1 lists parameter values that were changed to achieve validation. Note whereas twelve LOBULAR parameter adjustments were needed to validate DISEASED_{CCl4} ISL, only six were needed to validate DISEASED_{ALC} ISL. Except for the *C2BJumpProb* adjustments, the magnitude of the adjustments needed for DISEASED_{ALC} ISL was smaller than those of DISEASED_{CCl4} ISL. Overall, the parameter value changes are consistent with less profound and fewer observed pathological changes caused by alcohol pretreatment [1].

DILTIAZEM outflow profiles from each of the three ISLs are graphed in Fig. 3. SM values for unsmoothed profiles were 0.92 (NORMAL), 0.92 (DISEASED_{CCl4}), and 0.91 (DISEASED_{ALC}). SM values for smoothed data are listed in Fig. 3. Hereafter, unless stated otherwise, all results are reported in the order NORMAL, DISEASED_{CCl4} and, DISEASED_{ALC}, when values for all three are provided, and DISEASED_{CCl4} and DISEASED_{ALC} when only DISEASED ISL values are provided.

Previous studies have detailed how the generative consequences of ISL parameters are networked and nonlinear [2], [3]. A small change in one parameter can be offset by adjustments of other parameters. Consequently, studies of sensitivity to individual parameters are less informative and less meaningful than are location changes in ISL parameter space. Individually, the parameter changes in Table 1 did not cause statistically significant changes in outflow profiles. In general, a 5% change in any one parameter would not result in a visible change in outflow profiles. However, a 5% change in all parameters can cause a significant

Table 1. Parameter differences between NORMAL and DISEASED ISLs

Parameter	NORMAL	DISEASED_{CCl4}	DISEASED_{ALC}
A2BJumpProb	0.4	0.2	0.35
B2AJumpProb	0.37	0.3	0.37
B2CJumpProb	0.55	0.35	0.65
C2BJumpProb	0.45	0.55	0.25
ECDensity	0.65	0.06	0.65
HepDensity	0.70	0.65	0.70
SoluteBindProb	0.5	0.35	0.50
BinderPerCell	90	65	75
SoluteBindCycles	10	29	9
SSTypeRatio	20	100	20
DirSinCirc	24	22	24
SinusoidTurbo	0.82	0.85	0.82

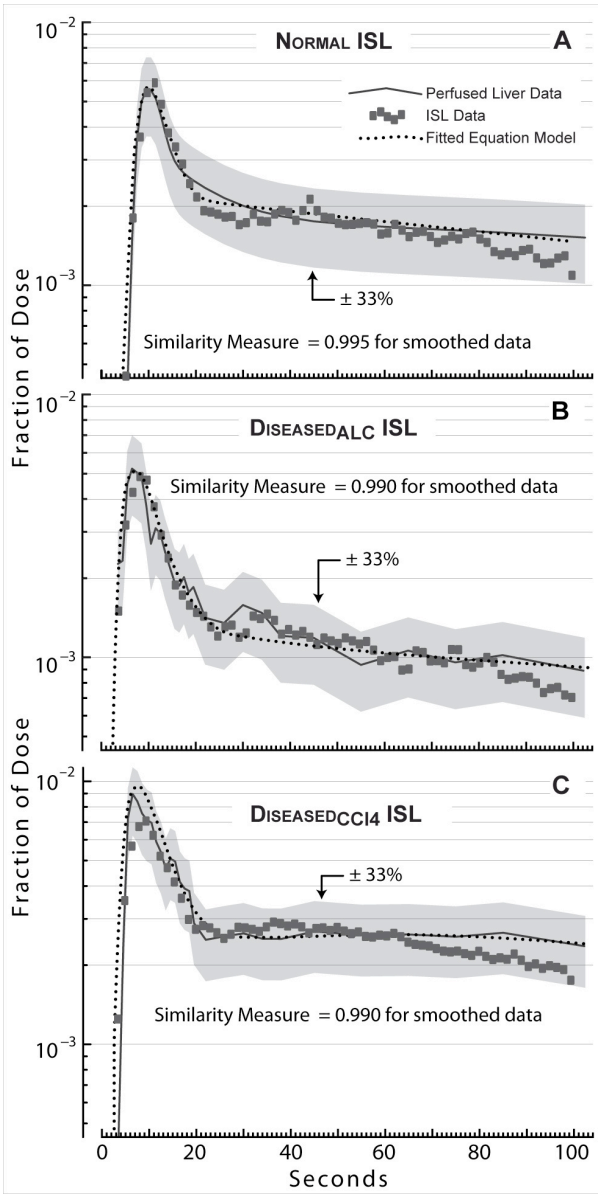

Figure 3. Outflow profiles of diltiazem in normal and diseased ISLs. Smoothed diltiazem outflow values are plotted for **(A)** NORMAL, **(B)** DISEASED_{ALC}, and **(C)** DISEASED_{CCl4} ISLs. They achieved validation by having Similarity Measure (SM) > 0.9. The SM computes the fraction of collected COMPOUNDS that lies within a band (± 33%) around the referent outflow values. ISL data shown are averages of 48 Monte Carlo runs. Solid lines connecting referent outflow data are graphed along with the output of the fitted mathematical model (dotted curves) [1].

change. The changes in Table 1 averaged 32% for DISEASED$_{CCl4}$ ISLs and 18% for DISEASED$_{ALC}$ ISLs.

4.2. Tracing DILTIAZEM Disposition

From raw DILTIAZEM tracing data, any number of derived measures can be obtained, and each enables viewing disposition from a different perspective. Each provides a somewhat different image of events occurring within ISLs during simulations. Some measures may be useful in helping us think about ISLs (e.g., what change may be needed during parameter tuning to move closer to targeted phenomena). Others may be helpful in thinking about hepatic disposition of the referent compound. Still others may be helpful in thinking about different disease consequences and even disease progression. Here we focus our analysis on DILTIAZEM movements within LOBULES, which highlight functional and structural differences between NORMAL and DISEASED ISLs.

Fig. 4 shows how stochastic DILTIAZEM movements within the three spaces influenced average DILTIAZEM resident TIMES. The bar graphs (Fig. 4A-C) specify the DOSE fraction having resident TIMES within the indicated ten-SECOND range. The three curves in Fig. 4D specify the fraction of dose having a LOBULE resident TIME equal to or less than the indicated TIME. For both DISEASED ISLs, there was a reduction in DILTIAZEM having 0–10 SECOND resident TIMES, and an increase in DILTIAZEM having 10–20 SECOND resident TIMES. The net effect for both DISEASED ISLs was an increase in DILTIAZEM having longer resident TIMES, which is evident in the bar graphs. The two DISEASE types altered resident TIME patterns differently (Fig. 4B,C). Surprisingly, there were no significant differences in mean (and SD) DILTIAZEM resident TIMES: 47.8 (26.0), 48.8 (25.2), and 45.9 (26.5) SECONDS. Several factors influenced the differences between resident TIMES. *A2BJumpProb* differences between the three ISL types (0.38, 0.21, and 0.35) caused fewer DILTIAZEM to move into Space B in DISEASED relative to NORMAL LOBULES. Similarly, differences in *B2CJumpProb* (0.55, 0.34, and 0.65) caused fewer of the DILTIAZEM that did reach Space B in DISEASED$_{CCl4}$ relative to DISEASED$_{ALC}$ to move into Space C.

The path length data shown in Fig. 4E-H are measures of the cumulative length of all SSs entered by each DILTIAZEM. All three LIVER types had 70 SSs distributed among the three zones. On average, NORMAL and DISEASED$_{ALC}$ LIVERS had 3.5 of the long, narrow SSs, whereas only occasionally did a DISEASED$_{CCl4}$ LIVER have even one. Consequently, a small subset of DILTIAZEM path lengths in NORMAL and DISEASED$_{ALC}$ LIVERS were long, but they were essentially absent in the DISEASED$_{CCl4}$ LIVERS. The SSs in Zone 1 map to the interconnections between sinusoids that are most numerous in the periportal region but are absent in the perivenous region of normal lobules. Microscopy evi-

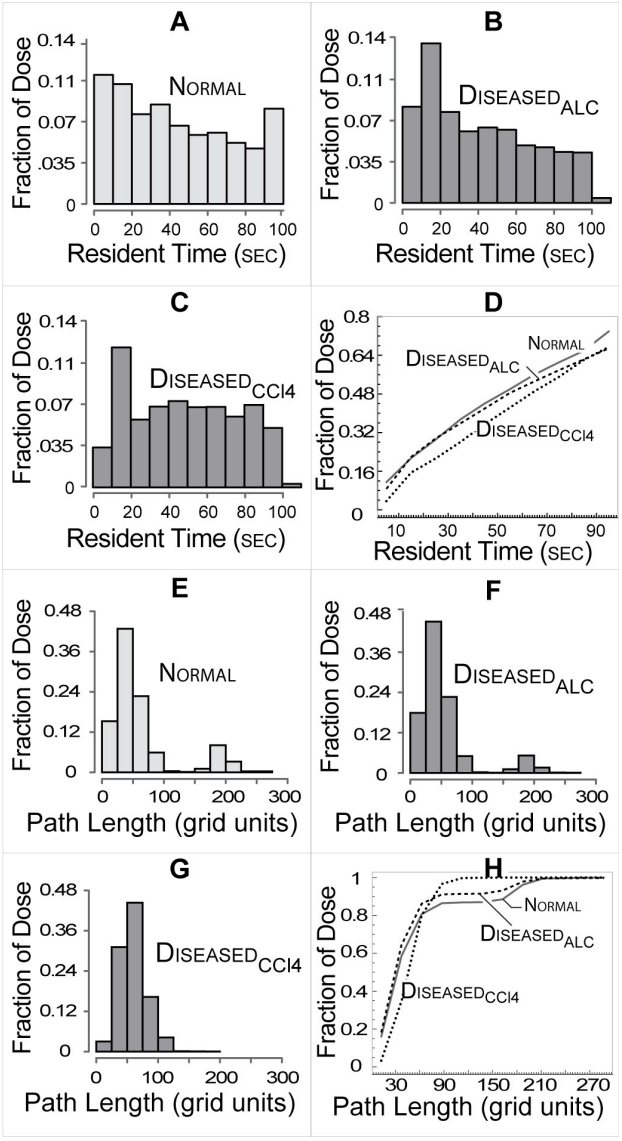

Figure 4. DILTIAZEM resident TIMES and traversal path lengths in NORMAL and DISEASED LIVERS. **(A-C)** Resident TIME measures the amount of TIME a DILTIAZEM resides in a LOBULE. Each DILTIAZEM was traced from initial injection until it was METABOLIZED, cleared from the LOBULE through the CENTRAL VEIN (CV), or the simulation run ended. Shown are average resident TIME histograms for (A) NORMAL, (B) DISEASED$_{ALC}$, and (C) DISEASED$_{CCl4}$ LOBULES. Bar heights measure the fraction of dose having resident TIMES within the indicated ten-SECOND interval. **(D)** Resident TIME curves represent cumulative sum of the heights of the bars in each of the three histograms. A point on each curve is the dose fraction that had resident TIME $\leq$ the indicated TIME. **(E-G)** Path length measures the total length (in grid units) of Sinusoidal Segments visited by a DILTIAZEM. Shown are average path length histograms for (E) NORMAL, (F) DISEASED$_{ALC}$, and (G) DISEASED$_{CCl4}$ LOBULES. Histogram bin size is 25 grid units. Bar height corresponds to fraction of administered DILTIAZEMS. **(H)** Path length curves represent the cumulative sum of the heights of the bars in each of the three histograms.

dence suggests that some of those interconnections are lost in CCl_4-treated, cirrhotic lobules [6].

We recorded each DILTIAZEM'S SINUSOID traverse path for 100 SECONDS after dosing: until it either exited the LOBULE, was METABOLIZED, or the run ended. Path lengths were divided into two types: complete and incomplete. In the above order, the mean percent of the dose that ended at CV was 47, 59, and 38%, whereas 23, 9, and 29% ended at a SS (and was METABOLIZED). Passage was still in progress when the run ended for 30, 32, and 33% of the DILTIAZEM dose. The average path lengths, in the above order, were 64, 59, and 55 (in grid units). The shorter mean paths for DISEASED ISLs show that both types of DISEASE made it easier for DILTIAZEM to move closer to CV as TIME advanced. It is evident from Fig. 4E-G that $DISEASED_{CCl4}$ ISLs had a more narrowly distributed variety of path lengths. Note also that the $DISEASED_{CCl4}$ ISLs had significantly fewer of the shortest paths (0–25 grid units) than either NORMAL or $DISEASED_{ALC}$ ISLs.

5. DISCUSSION

For the level of abstraction used, the ISL outflow results support the idea that both mechanism and event level mappings in Fig. 1 may be reasonable. The incremental parameter changes that were necessary (and sufficient) to transform a NORMAL liver into a DISEASED LIVER may correspond abstractly to molecular, cellular, and sinusoid level transformations responsible for the pathogenesis from normal into diseased livers during CCl_4 and alcohol treatment. The general consistency between DISEASED LIVERS during execution and the cited histopathology evidence supports the hypothesis. We thus have a tentative, yet promising, in silico model that enables us to visualize, abstractly from the perspective of diltiazem, how the consequences of cirrhosis may have progressed. That new capability represents an important step toward unraveling the complex influences of disease on drug disposition.

Being able to transform one validated model into another is important. Having independently validated NORMAL and DISEASED LIVERS allows one to explore plausible drug disposition consequences of intermediate levels of disease and even disease that is more advanced. Because of individual differences in disease progression, conducting wet-lab experiments to document the former would be problematic, and the latter may be deemed unethical. By assuming disease progression corresponds to gradual change from NORMAL to DISEASED LIVER parameter values, we can simulate a liver that has progressed half way, for example, along the path to the currently documented disease state. We can project further parameter changes to explore plausible consequences of more advanced level of disease. Corresponding explorations of intermediate and advanced disease states would be infeasible using traditional inductive mathematical models. Ultimately, the approach can facilitate rational translation of research results to useful applications, and that may open doors to development of strategies for tailoring drug choices to help reverse disease conditions.

Making progress toward the long-term goals requires more sophisticated, detailed features. One such feature pertains to SS graphs, which, in current implementation, are abstract, randomized networks of SS nodes that have no concrete mapping to the spatial structure of sinusoids within referent liver lobules. For this study, because outflow profiles were our validation data, there was no need to make LOBULES explicitly spatial. Adding such a requirement merely for the purpose of making the structure of the LOBULE more intuitive or "more like" the referent, absent any fine-grained spatial data against which to validate, runs counter to the parsimony guideline. On the other hand, there is some reasonable pressure to make the LOBULES spatially explicit. Lobular zonation and sinusoidal structure data exist and are explicitly spatial [8], [9]. Because current LOBULES can contain graphs that cannot project onto a 3D vector space, validation against such zonation data is infeasible. Doing so would be more straightforward if the ISL LOBULES were spatially explicit. We are considering making them so in future experiments.

The iterative modeling and experimentation process is an integral part of ISL development [2], [5]. That process involves continual evaluation and testing of the model and implementation details, which helps build a degree of confidence in the model accuracy (i.e., verification). For this study, we started with ISLs that have been extensively tested and scrutinized to insure achievement of prespecified Similarity Measure values. Because the transformation from NORMAL to DISEASED LIVERS did not involve changes to the actual implementation, model verification was not a central focus herein. Moving forward, the continual, rigorous model verification will be critical to insuring confidence as existing ISL features are modified or new details added.

6. IMPLEMENTATION TOOLS

System framework was implemented using Swarm 2.2 (www.swarm.org) on a small-scale Beowulf cluster system consisting of one master node and seven client nodes. Simulation and tracing results were analyzed using R 2.7.1 (www.r-project.org) and MATLAB (www.mathworks.com).

ACKNOWLEDGMENTS

We thank Michael Roberts at University of Queensland Australia and members of the UCSF BioSystems group for helpful suggestions and discussions. We gratefully acknowledge research funding provided by the CDH Research

Foundation and a graduate fellowship to SK from the International Foundation for Ethical Research. A manuscript containing the results presented herein plus additional observations has been submitted to Annals of Biomedical Engineering.

REFERENCES

[1] Hung, D.Y.; P. Chang; K. Cheung; B. McWhinney, P.P. Masci; M. Weiss; M.S. Roberts. 2002. "Cationic drug pharmacokinetics in diseased livers determined by fibrosis index, hepatic protein content, microsomal activity, and nature of drug." J. Pharmaco. Exp. Ther. 301(3): 1079-1087.

[2] Park, S.; G.E. Ropella; S.H.J. Kim; M.S. Roberts; C.A. Hunt. 2009. "Computational strategies unravel and trace how liver disease changes hepatic drug disposition." J. Pharmaco. Exp. Ther. 328(1): 294-305.

[3] Yan, L.; G.E.P. Ropella; S. Park; M.S. Roberts; C.A. Hunt. 2008. "Modeling and simulation of hepatic drug disposition using a physiologically based, multi-agent in silico liver." Pharm. Res. 25: 1023-1036.

[4] Schiff, E.R.; M.F. Sorrell; E.C. Maddrey (editors). 2003. Schiff's Diseases of the Liver. 9th Edition. Lippincott, Williams & Wilkins, Philadelphia, PA.

[5] Hunt, C.A.; G.E.P. Ropella; L. Yan; D.Y. Hung; M.S. Roberts. 2006. "Physiologically based synthetic models of hepatic disposition." J. Pharmacokinet. Pharmacodyn. 33(6): 737-772.

[6] Gaudio, E.; P. Onori; A. Franchitto; R. Sferra; O. Riggio. 1997. "Liver metabolic zonation and hepatic microcirculation in carbon tetrachloride-induced experimental cirrhosis." Dig. Dis. Sci. 42(1): 167-177.

[7] Siebert, G.A.; D.Y. Hung; P. Chang; M.S. Roberts. 2004. "Ion-trapping, microsomal binding, and unbound drug distribution in the hepatic retention of basic drugs." J. Pharmacol. Exp. Ther. 308: 228-235.

[8] Gebhardt, R. 1992. "Metabolic zonation of the liver: Regulation and implications for liver function." Pharmacol. Ther. 53: 275-354.

[9] Jungermann, K. 1995. "Zonation of metabolism and gene expression in liver." Histochem. Cell. Biol. 103: 81-91.